Pergamon

Deep-Sea Research I, Vol. 41, No. 4, pp. 603–628, 1994

0967–0637/94 $7.00 + 0.00

Mesoscale circulation and thermohaline structure of the Black Sea observed during HydroBlack '91

T. Oguz,* D. G. Aubrey,† V. S. Latun,‡ E. Demirov,§ L. Koveshnikov,‡ H. I. Sur,* V. Diaconu,‖ S. Besiktepe,* M. Duman,¶ R. Limeburner† and V. Eremeev‡

(*Received* 16 *February* 1993; *in revised form* 13 *August* 1993; *accepted* 1 *September* 1993)

Abstract—Results from nearly 300 hydrographic stations occupied during HydroBlack '91, a basin-wide survey performed during September 1991, reveal a complex, eddy-dominated three-dimensional circulation in the Black Sea. Except in the areas of anticyclonic eddies distributed around the periphery of the basin, the inshore portion of the Rim Current along the relatively smooth continental margin topography forms a narrow coastal jet characterized by small amplitude (~20–30 km) undulations with a wavelength of ~125 km. The offshore margin of the Rim Current, however, exhibits large meanders, offshore filaments and dipole eddy structures. The Rim Current is accompanied by a strong frontal zone having cross-frontal temperature and salinity differences of ~1.0°C and ~0.5, respectively, near the surface. The circulation within the interior of the sea is composed of an interconnecting series of cyclonic eddies and gyres, varying in size and shape with depth. The mesoscale variability introduces a different scale of complexity to the general circulation at each pressure level, although larger and quasi-persistent features of the general circulation are fairly coherent down to 500 dbar. Important structural changes, however, take place in both large scale and mesoscale components of the circulation at 500 dbar and deeper, consistent with the findings of the September 1990 survey (Oguz *et al.*, *Deep-Sea Research I*, **40**, 1597–1612). The circulation is strongest in the upper layer (~150 dbar), where the calculated geostrophic currents have speeds of 0.2–0.3 ms^{-1} along the axis of the Rim Current. The strength, width, and frontal intensity of the Rim Current, however, reduce considerably below the permanent pycnocline.

1. INTRODUCTION

The Black Sea is a nearly-enclosed marginal sea possessing many of the processes and features of major ocean basins but lacking some of the complexities that make it difficult to understand and to study. Notable features of this basin include the lack of an open boundary (making it simpler to model), and the combination of wind stress and buoyancy forcing together with water mass formation and lateral exchange of mass through the Bosphorus driving the complex flows. The basin is nearly anoxic, with only the upper 150 m of the total 2200 m water depth possessing measurable oxygen; the deep waters are rich

*Institute of Marine Sciences, Middle East Technical University, Erdemli, Turkey.
†Woods Hole Oceanographic Institution, Woods Hole, MA 02543, U.S.A.
‡Marine Hydrophysical Institute, Sevastopol, Ukraine.
§Institute of Oceanology, Varna, Bulgaria.
‖Romanian Marine Research Institute, Constantza, Romania.
¶Institute of Marine Science and Technology, Dokuz Eylül University, Izmir, Turkey.

in hydrogen sulfide. A permanent halocline separates the oxic and anoxic waters; a seasonal thermocline at 15–30 m depth provides another sharp density gradient affecting the baroclinic processes. The biogeochemical cycling in this basin is notably different from open oceans, posing interesting problems for oceanographers of all disciplines. Recent studies confirm this interest (e.g. Murray, 1991; Izdar and Murray, 1991). Many eastern European scientific books and articles attest to broad scientific interest in the Black Sea, but these are less known by most scientists.

The Black Sea is characterized by a predominantly cyclonic and strongly time-dependent and spatially structured basin-wide circulation (Filippov, 1968; Sorokin, 1982; Blatov *et al.*, 1984; Stanev *et al.*, 1988). The Rim Current flowing along the abrupt continental slope and margin topography, one or more cyclonic gyres occupying the interior portions of the basin, and a series of anticyclonic eddies confined inshore of the Rim Current have been reported to constitute major seasonal/interannual components of the circulation (see discussion given by Oguz *et al.*, 1993; Fig. 4 in Eremeev *et al.*, 1992). Using climatological data, the quasi-permanent, larger scale elements of the circulation have been shown to undergo structural variability on a monthly time scale (Eremeev *et al.*, in press; Trukhchev and Demin, 1992). The Rim Current frontal zone has important implications for the biogeochemistry of the Black Sea. It can essentially form a biogeochemical barrier between coastal and offshore waters, at times isolating interior basin waters from the more polluted coastal waters. The ecosystem of the coastal zone is very different to just offshore of the frontal zone, and is characterized by much higher plankton and suspended organic material concentrations (Sapozhnikov, 1991).

Recent studies involving satellite observations (Kazmin and Skliarov, 1982; Oguz *et al.*, 1992) indicate that the Rim Current exhibits meanders and cross-stream jets forming a dominant and persistent component of the general circulation. Offshore jets extend more than 100 km from the shelf break and have peak velocities of about 70 cm^{-1} (Ivanov *et al.*, 1985). They appear to have no preferred locations for their formation and are more common during summer and autumn. The mesoscale imprint on the circulation inferred from satellite images is also supported by a limited number of regional hydrographic surveys performed at mesoscale resolution (e.g. Latun, 1990). The onshore–offshore excursions of the highly convoluted frontal boundary and mesoscale features must link the biogeochemical processes in the coastal regions to those within the interior of the sea beyond the continental margin, and therefore provide a mechanism for two-way heat, salt and material transports between nearshore and offshore regions. Although cross-slope exchange is inhibited for many geometries, the Black Sea conditions enhance such exchange.

The Black Sea, with mesoscale dynamics and interactions taking place over a relatively small Rossby radius (~20–30 km), provides a suitable environment to carry out synoptic scale investigations with mesoscale resolution. Furthermore, because the ecology of the basin has undergone severe changes due to human influences (Aubrey *et al.*, 1992a; Mee, 1992), it provides an opportunity to study the interaction between physical processes and biogeochemical processes. Motivated by the general lack of high resolution (both vertically and horizontally), regional data on its circulation, thermohaline and biochemical characteristics, as well as the serious ecological and environmental problems requiring immediate attention, a cooperative scientific research program (the Cooperative Marine Science Program for the Black Sea—CoMSBlack) was formed to initiate coordinated, multi-institutional, interdisciplinary research efforts between the neighboring countries

(see AUBREY *et al.*, 1992a, for details). The HydroBlack '91 cruise constitutes the first basin-wide, multi-ship operation realized within the framework of this program. It was organized to obtain a basin-wide description of the circulation, thermohaline and biogeochemical characteristics of the Black Sea, to determine the spatial distribution of important physical and biogeochemical parameters, and to investigate their interrelations with mesoscale features (eddies, jets and filaments). A complete data set was acquired for the first time for the entire sea with the participation of five ships and scientists from four riparian countries and the U.S.

This paper focuses on the circulation characteristics and associated water property distributions obtained from the HydroBlack '91 data set, with special emphasis given to their mesoscale spatial variability. A brief description of field measurements and the data analyses is provided in Section 2. The baroclinic flow field and associated thermohaline structure are described in Section 3 by means of the dynamic height, temperature and salinity fields at selected pressure levels, and their vertical structures along various cross-sections, after a brief description of the basic water mass characteristics. Finally, discussion and conclusions are provided.

2. FIELD MEASUREMENTS AND DATA ANALYSES

The HydroBlack '91 survey was accomplished using two Ukrainian vessels (R.V.s *Prof. Kolesnikov* and *Parshin*), two Turkish vessels (R.V.s *Bilim* and *K. Piri Reis*), and one Bulgarian vessel (R.V. *Akademik*) between 2 and 29 September 1991 (Table 1). The station network was comprised of approximately 300 stations, and different ships had different areas of responsibility (Fig. 1). Except in the wider western and northwestern shelves, most stations are located in the deeper part of the basin, the inshore edge of the grid laying along the upper continental slope (about 500–1000 dbar). Resolution of the spatial structure of the energetic hydrographic fields was attempted by the choice of ~20 nm (~36 km) station spacing, which was constrained by the need to accomplish the survey synoptically at reasonable resolution. However, because the survey took about 4 weeks to complete, temporal variability within this period has aliased the horizontal property distributions. AVHRR images taken throughout the measurement period clarify some of the time-varying evolution of surface temperature during this interval of measurement.

During the survey the synoptic weather conditions were characterized by the passage of two consecutive low and high pressure systems, each having a period of 4–7 days. The low pressure systems were accompanied by intensification of westerly winds and heavy precipitation. The mean air temperature, relative humidity and wind speed during the entire survey were about 20°C, 70% and 5 m s^{-1}, respectively.

Table 1. *Cruise inventory for HydroBlack* '91

Vessel	Country	Dates
R.V. *Akademik*	Bulgaria	2–12 Sept. 1991
R.V. *Bilim*	Turkey	5–23 Sept. 1991
R.V. *Koca Piri Reis*	Turkey	7–17 Sept. 1991
R.V. *Parshin*	Ukraine	8–12 Sept. 1991
R.V. *Prof. Kolesnikov*	Ukraine	9–29 Sept. 1991

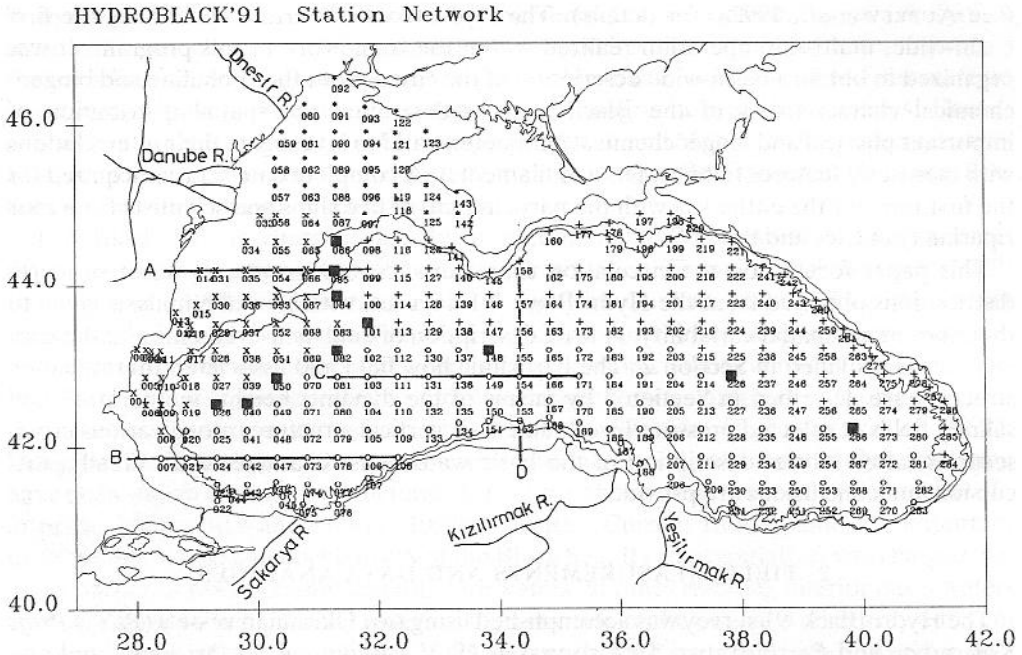

Fig. 1. Station network and bathymetry of the Black Sea, showing transect lines referred to in text. Symbols denote different ships used in the cruise: ○, *Bilim* and *Piri Reis*; +, *Kolesnikov*; x, *Akademik*; *, *Parshin*. Bathymetry includes 200 and 1000 m contours. Squares denote intercalibration stations.

The hydrocasts on the R.V. *Bilim*, R.V. *Akademik* and the R.V. *K. Piri Reis* were made using Sea-Bird SBE9 CTD profilers, having an accuracy of about +0.003°C in temperature and +0.0004 Sm^{-1} in conductivity. The R.V. *Prof. Kolesnikov* was equipped with the Istok 5 CTD system having accuracies of about +0.025°C and +0.00025 Sm^{-1}. The R.V. *Parshin* measurements, performed in the relatively isolated semi-enclosed shelf region approximately north of 45°N, were initially taken with the SBE19 CTD unit until its pressure sensor failed halfway through the cruise. The remaining data were taken with a coarse-resolution instrument (Hydrozond) which had problems with its conductivity cell.

The CTD casts were made to a nominal depth of 1000 dbar, but deeper measurements to the bottom were performed at one-third of the stations located in the central Black Sea where the depth is approximately 2000 m. The CTD data were put into one dbar bin-averaged form, then intercalibrated and pooled during an Intercalibration Workshop held at the Woods Hole Oceanographic Institution during 1–10 December 1991 (Aubrey *et al.*, 1992b). Filtering and spike removal were first applied to several stations of the R.V. *Akademik* and the R.V. *Prof. Kolesnikov* data before the intercalibration. The filtered and de-spiked data sets were then compared at a series of common stations (Fig. 1) acquired independently by at least two ships. The intercalibration was performed both on the temperature and conductivity by comparing their values in the bottom boundary layer (~400 m thick) possessing practically uniform T, S properties (Murray *et al.*, 1991). Based on these comparisons, the temperatures for the R.V.s *Bilim*, *K. Piri Reis* and *Akademik* data sets were intercalibrated. The R.V. *Prof. Kolesnikov* temperature was reduced by

0.01°C, although the scatter about this value was about 0.005°C. The conductivity values of the R.V.s *Bilim* and *Akademik* were nearly equal (within approximately 0.006 Sm^{-1} of each other); the rest of the data was intercalibrated with respect to these. The *Kolesnikov* and *K. Piri Reis* conductivities were reduced by 0.023 Sm^{-1} and 0.01 Sm^{-1}, respectively. The *Akademik* conductivity also was reduced by 0.006 Sm^{-1}, which was close to the accuracy of the present data.

The agreement of the intercalibrated data sets was better than 0.01°C in temperature and 0.004 in salinity calculated from the corrected temperature and conductivity values. The potential temperature and potential density were then computed; together with pressure and salinity, these formed the basis for subsequent analyses. In addition, geopotential anomalies (dynamic heights) relative to 900 dbar were calculated at selected pressure levels to delineate the distribution of the geostrophic flow in the basin. Stations on the shelf and upper continental slope (at depths shallower than 900 dbar) were not included into the dynamic height computations. The presence of weak currents below the upper layer (>~150 dbar), typical of the Black Sea subhalocline waters (Titov, 1980; Trukhchev and Demin, 1992), makes the calculated geostrophic currents and their transports relatively insensitive to the choice of reference depth. In the present analysis, the geopotential anomaly values are normalized by the gravitational acceleration, and thus provide essentially sea-level heights in units of centimeters.

Sea-level height topography (SLHT) maps and horizontal property distributions presented in the following sections are based on subjective analysis and hand-contouring. The objectively mapped station data contoured by computer-based routines available to us were able to provide only smoothed fields of larger scale features, but did not represent adequately the mesoscale structures (Fig. 4a and b).

A series of AVHRR images was analysed with the hydrographic data, although some cloud cover obscured the area. The surface features observed in the AVHRR imagery were used to interpret the mesoscale structure of the Black Sea. Correlations of AVHRR temperatures and observed temperatures were qualitatively good. The AVHRR images also enabled us to investigate the time evolution of the surface features, since HydroBlack data were not taken synoptically, but were rather spread over a 4-week interval of time. These satellite data provide a way to evaluate qualitatively the aliasing caused by the non-synopticity of the water column observations.

3. BAROCLINIC FLOW AND THERMOHALINE STRUCTURE

3.1. *Water mass characteristics*

The water mass structure of the sea during the survey period was characterized by strong thermal stratification and considerable differences between the cyclonic and anticyclonic regions, particularly in the upper 200 dbar, with diminishing contrasts below. Figure 2 shows the cruise-average temperature, salinity and density profiles together with the profiles for Stas 227 and 272, representative of the cyclonic and anticyclonic regions, respectively. Temperature differences as large as ~2°C, salinity and density anomaly differences up to 0.5 and 1 kg m^{-3} are observed in the shallow isothermal and isohaline surface layer. The relatively uniform properties of the surface mixed layer overlie steep gradients of the seasonal pycnocline–halocline–thermocline system. This transition zone has a thickness of ~5 dbar centered at ~15 dbar in the cyclonic regions and at ~25 dbar in the anticyclonic regions. Across this zone, the mean density anomaly σ_θ changes from 12.0

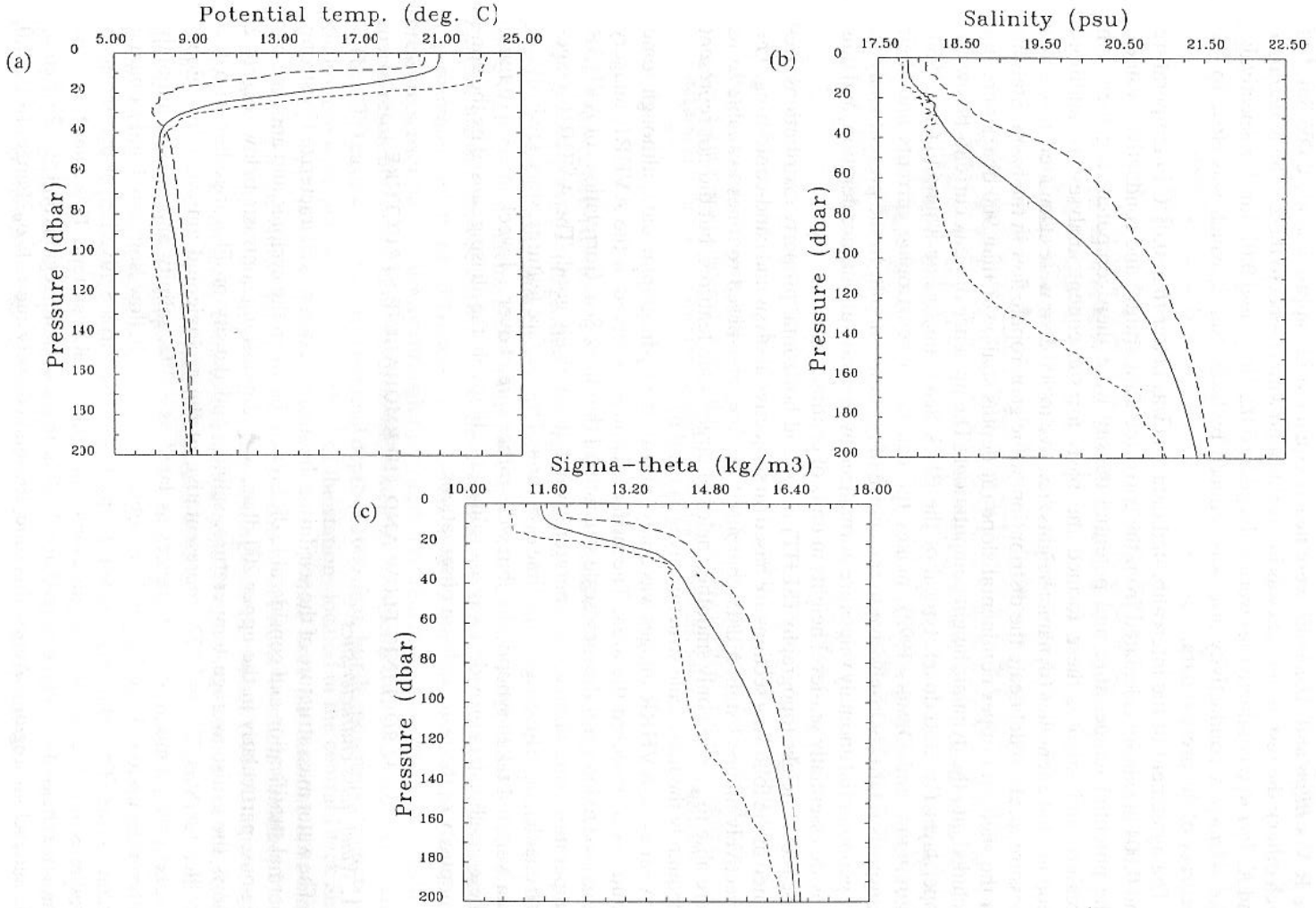

Fig. 2. Potential temperature, salinity, and σ_θ profiles from surface to 200 dbar level for three situations: ——— basin-wide average; — — — cyclonic

to 14.0 kg m^{-3}, the mean salinity increases from about 17.9 to 18.3, and the mean temperature decreases from about 22 to 10°C.

Below the seasonal thermocline–halocline–pycnocline is another layer of strong temperature stratification, the Cold Intermediate Layer (CIL). The CIL, identified by temperatures less than 8°C, starts immediately below the seasonal thermocline and extends to ~100 dbar. The cruise-average minimum temperature of ~7.2°C occurs at ~45–50 dbars, corresponding to the density surfaces σ_θ~14.4–14.5 kg m^{-3}. This temperature minimum is accompanied by a nearly linear increase in the salinity and density anomalies to about 20.2 and 15.6 kg m^{-3} at its lower boundary of ~100 dbar.

The CIL water is relatively fresher (1) and less dense (1 kg m^{-3}), though cooler, in the anticyclonic regions compared to the cyclones. In the cyclonic regions, the CIL is thinner and confined to shallower depths immediately below the seasonal thermocline. Its upper boundary is located at a depth of ~20 dbar, having a typical thickness of ~40 dbar. In the anticyclonic regions, the position of the upper boundary is at ~40 dbar with a thickness of ~120 dbar. Irrespective of the variations in the flow structure, the upper and lower boundaries of the CIL correspond to σ_θ~14.15 kg m^{-3} and σ_θ~15.65 kg m^{-3} isopycnal surfaces.

Below the CIL, a layer forming the base of the permanent pycnocline has mean salinity, potential temperature, and density anomaly increasing almost linearly to 20.8, 8.5°C, 16.2 kg m^{-3}, respectively, to a depth of ~140 dbar (Fig. 2a). This part of the pycnocline is known as the Suboxic Layer (hereafter referred to as SOL), characterized by specific oxygen–nitrate, H_2S–phosphate correlations at their upper (σ_θ~15.4 kg m^{-3}) and lower (σ_θ~16.2 kg m^{-3}) surfaces, respectively (Tugrul *et al.*, 1992; Saydam *et al.*, 1993). Murray (in press).has proposed the σ_θ = 15.65 kg m^{-3} surface as the upper bound for the SOL, based on pumpcast data taken during 1988 R.V. *Knorr* cruises. Since this surface lies within the pycnocline, the vertical difference between 15.40 and 15.65 density levels is about 5 m. If 15.65 is chosen as the upper surface, it coincides with the lower boundary of the CIL. The SOL is also identified as the zone of maximum mesoplankton concentration (Vinogradov *et al.*, 1990). Analogous to the CIL, the SOL is also thinner and confined to shallower depths in the cyclonic regions.

Below the base of the SOL lie the intermediate and deep layers in which the temperature and salinity increase more gradually but uniformly with depth. The deep layer is underlain by a bottom mixed layer having an average thickness of 400 dbar and vertically uniform properties. The *T–S* characteristics of the lower layer waters below the permanent pycnocline are described by Murray *et al.* (1991).

Temperature inversions associated with intrusion of Mediterranean underflow into the ambient Black Sea waters within the intermediate depths (100–500 dbars) are a characteristic feature of the southwestern Black Sea water mass structure. The mixing characteristics of the Mediterranean waters in the Black Sea have been explored recently in a number of papers (Latif *et al.*, 1990; Oguz *et al.*, 1991; Özsoy *et al.*, 1991; Oguz and Rozman, 1991), and therefore will not be repeated here. Several examples are shown in Fig. 3.

3.2. *Property distributions*

Near-surface fields. The 5 dbar SLHT map and corresponding baroclinic flow field (Fig. 4) illustrate the dominant features of the circulation field above the seasonal thermocline:

gyre (Sta. 227); ----- anti-cyclonic gyre (Sta. 272).

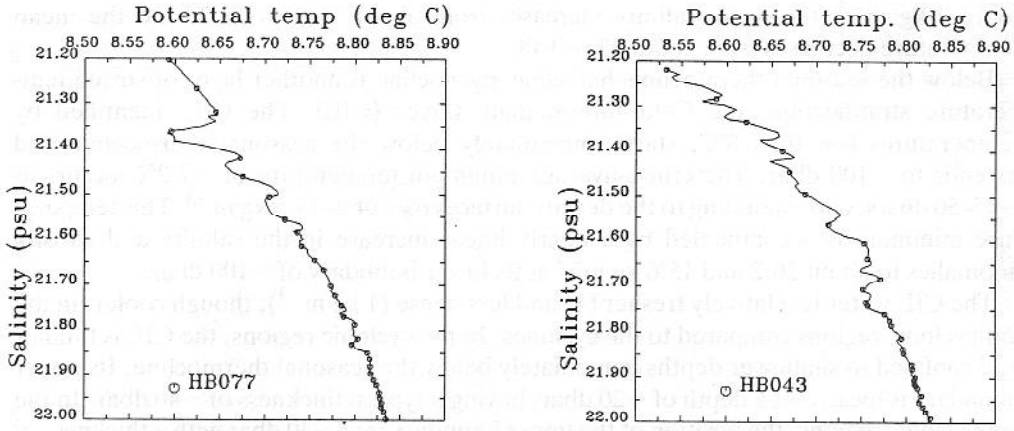

Fig. 3. Potential temperature versus salinity for two stations showing Mediterranean water intrusion into the Black Sea's southwestern corner.

a coastal current system and associated meanders, pronounced offshore jets as well as mesoscale eddies distributed all around the basin. Figure 4a,b reveals three distinct zones identified by three distinct ranges of geopotential anomaly contours. Those between +4 and −2 cm encircle the basin by following closely the steep topographic slope (see Fig. 1), and form the inner part of the Rim Current. This zone has a width of about 50 km and includes the strongest currents of the basin (>20 cm s^{-1}) with a maximum value of 33 cm s^{-1} (Fig. 4c). Along the southern coast, the current exhibits a wavy pattern with a length scale of about 125 km and amplitude <20 km. Along the northern coast the current possesses larger meanders having wavelength of about 250 km and amplitude of >25 km. These meanders are located to either side of the tip of the Crimean peninsula and along the central part of the Caucasian coast.

The SLHT contours denoted by −3 and −4 cm in Fig. 4a form the offshore extension of the Rim Current along the smoothly varying but abrupt continental margin topography and represent a series of large protrusions towards the interior around the basin. Along the southern coast, four of these mesoscale features are situated between approximately 31.5° and 35.5°E longitude, with their stems extending obliquely offshore in the upstream direction from the crests of these coastal "waves". In the discussion to follow, these filaments will be called by F1, F2, F3, F4 from west to east, respectively. Along the northern coast, a backward, cyclonically-curling offshore jet (F5) is observed as an offshore continuation of the intense Rim Current meandering, off the Sea of Azov. This is the most pronounced intrusion feature of the Rim Current in the Black Sea, and leads to formation of a dual-lobed cyclonic gyre tilted towards the northeast.

Although the SLHT contours between +4 and −4 cm represent the Rim Current, those smaller than −4 cm and those greater than +4 cm define, respectively, the cyclonic circulation of the basin's interior and the anticyclonically-dominated inshore region having a series of eddies described and named earlier by OGUZ *et al.* (1993). The so-called Batumi Eddy is the largest and strongest of these anticyclones and occupies the region to the east of 39°E longitude. Along the northern coast, the anticyclones are more pronounced and are associated with the intense meandering of the Rim Current. They will be called here, as in OGUZ *et al.* (1993), the Caucasian, Crimean and Sevastopol Eddies, from east to west. The

geostrophic current, in excess of about 20 cm s^{-1} along the periphery of these eddies, has a relatively stronger flow along the northern coast (Fig. 4c). Three anticyclonic eddies of the southern coast are relatively weaker and smaller. Those centered along 31° and 36°E longitude were identified in OGUZ *et al.* (1993) as the Sakarya and Kizilirmak Eddies. The anticyclonic eddy situated along the relatively smooth topographic slope along the western coast off Cape Kaliakra, Bulgaria, is termed the Kaliakra Eddy.

The circulation within the interior of the basin, expressed by SLHT contours less than −4 cm, is characterized by four isolated cyclonic eddies, separated by the offshore filaments of the Rim Current. The largest of these eddies is extended meridionally in the central part of the eastern basin and has two centers, both of which attain stronger circulation than the others. This cyclonic gyre is decoupled from the others in the central and western parts of the basin by filaments F5 and F4, off the Sea of Azov and Cape Sinop, respectively.

The 5 dbar salinity (S), potential temperature (Q), and density (σ_θ) fields representing the properties of the upper mixed layer above the seasonal thermocline are shown in Fig. 5. The near-surface salinity map (Fig. 5a) reveals almost all features of the 5 dbar circulation pattern. The anticyclonically-dominated coastal zone around the basin is characterized by relatively fresher waters having salinities less than 17.6, whereas the cyclonic eddies of the interior are identified by salinities greater than 18.0, the maximum value being about 18.2. The waters in the Rim Current attain intermediate salinity values between 17.6 and 17.9. The filaments advect the lower salinity coastal waters offshore, giving rise to patchy distributions of lower salinity waters within the basin's interior.

Salinity distributions along the southern and western coasts show regional variability due to local fresh water inflow. Along the southern coast, in the continental shelf areas off the Sakarya River mouth (~31°E) and off the Kizilirmak and Yesilirmak River mouths (~36°E), the salinities locally drop to values of 17.1–17.2. Along the western coast, the substantial fresh water input from Danube, Dniester, and Dnieper rivers generates a sharp salinity front, separating the lower salinity ($S < 17$) shelf waters from more saline ($S > 17.5$) interior waters. The front associated with the riverine flow is confined to the shallow surface mixed layer, and does not extend below the seasonal thermocline–halocline–pycnocline system (Fig. 6). The surface salinity is ~14.5 to the north of 44°N, increasing gradually to 16.5 southwards toward the Bulgarian coast. To the south of 42°N, the fresh shelf waters thin. The characteristic salinity of the southwestern shelf area is ~17.0. The relatively weak cross-frontal temperature differences imply that the front is dominantly a salinity front (Figs 5b and 6).

The 5 dbar salinity map provides additional details of the flow structure near the western and northwestern shelves that are not seen in the corresponding dynamic height field since the latter map is based on stations deeper than the depth of the assumed level of no-motion (900 dbar). Salinity mirrors the southward flow along the outer shelf associated with the strong horizontal density gradient. When combined with the Rim Current flowing along the continental slope, they form the strongest current system (~30 cm s^{-1}) in the Sea (see Fig. 4c). The small amplitude undulations observed along the western boundary of the basin in Fig. 4a emerge in the salinity map as large amplitude frontal variations extending all the way to the Sakarya Eddy region. The Kaliakra Eddy appears to be part of an intense frontal meander extending in a northwest–southeast direction.

The 5 dbar temperature distribution (Fig. 5b) reveals large temperature gradients in the

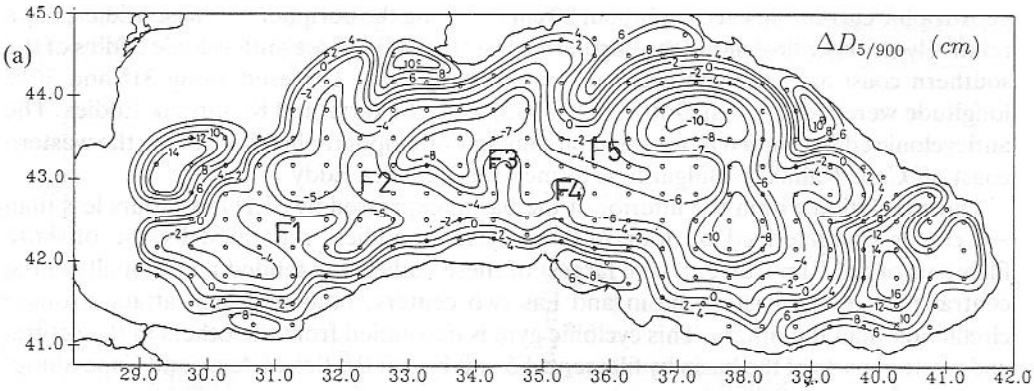

(b) 5/900 dbar Dynamic Height Topography

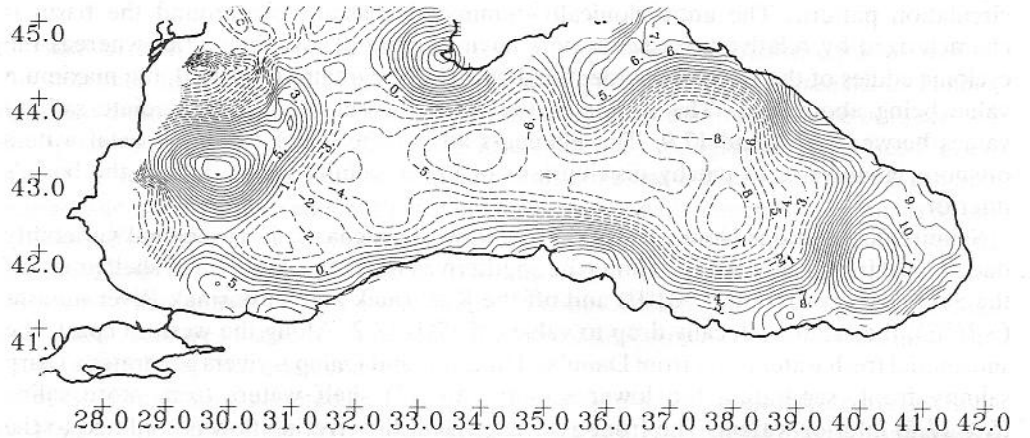

(c) 5 dbar geostrophic currents

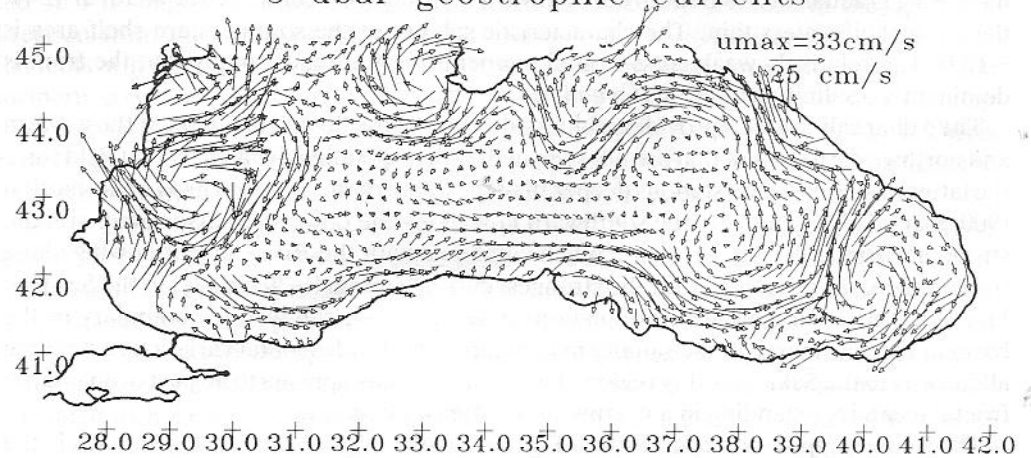

basin. The coldest waters ($\theta < 19°C$) occur within the cyclonic eddies to the south of the Crimean Peninsula and near the Caucasian coast up to 38°E longitude. These two colder spots are separated by the relatively warmer ($\theta \sim 20.5°C$) waters of filament F5, originated possibly within the Sea of Azov. This relatively colder and less saline coastal water mass partially intrudes towards the interior of the basin under the lighter water masses surrounding the filament. The temperature increases towards the eastern end of the basin, and attains its highest values ($\theta > 23°C$) within the central part of the Batumi Eddy. The coastal waters in the rest of the basin are identified by $\theta = 21$–$22°C$.

An anomalous feature of the temperature distribution is the relatively warm spot ($\theta \sim 22°C$) within the center of the western basin. This is separated from the colder spot ($\theta \sim 19°C$) to the south of the Crimean Peninsula by a temperature front extending in a northwest–southeast direction. The warm spot is separated by two weaker fronts from the meander of the Rim Current on its northwestern flank and from the cyclonic eddy on its southern flank. This warm spot might be a detached parcel of the warmer shelf waters extruded towards the interior of the western basin, although its salinity does not match that of the fresher coastal waters. The remaining features of the surface temperature field are consistent with the patterns of the surface salinity and SLHT fields.

The 5 dbar density map (Fig. 5c) reflects the major features of the corresponding salinity and temperature maps. The tongue of low salinity, warmer coastal water extending offshore from the Rim Current emerges as a band of less dense water ($\sigma_\theta \sim 11.0$–11.6 kg m^{-3}) along the southern and Caucasian coasts. The density front, however, becomes weaker and narrower along the central part of the northern coast in the relatively cold water mass. Inshore of the Rim Current the density anomaly generally attains values of 10.7–10.8 kg m^{-3}. The density front along the western coast is characterized by density anomaly variations of ~3.0 kg m^{-3} within a distance of ~50 km. The surface density anomaly exceeds 11.8 kg m^{-3} within the basin's interior.

Subsurface fields. The baroclinic velocity field varies considerably with depth both for intensity and form of the Rim Current, as well as for the flow structure within the interior of the basin. Salinity transects (Figs 7 and 8) indicate that the filaments F1 to F4 observed at the 5 dbar SLHT map, are confined essentially to the surface mixed layer with gradually diminishing signature towards the subsurface. At 100 dbar, the circulation within the interior of the basin becomes much simpler, and is dominated by a single elongated cyclonic cell (Fig. 9a). This cyclonic cell is intruded only by filament F5, giving rise to two separate cyclonic eddies in the eastern part of the basin. The width of the Rim Current, identified by SLHT contours $-1 < \Delta D < 2$ cm, is comparable to that at the surface. The typical current speed is about 10 cm s^{-1} along the main axis of the Rim Current, with strongest currents of 25 cm s^{-1} adjacent to the western shelf-break.

Another modification observed in the 100 dbar and deeper circulation fields is the formation of a new filament extruded from the southwesterly-flowing Rim Current along the western part of the basin. This filament (F6), identified by $\Delta D = -2$ cm contour in Fig. 9a, extends eastward along ~42.5°N. Its formation appears to be related with filament F1,

Fig. 4. (a) Sea-level height (cm) topography map at 5 dbar relative to 900 dbar level, hand-contoured using AVHRR images to define mesoscale features. (b) Same as (a), but contoured objective analysis results of CTD data only. (c) Geostrophic currents (cm s^{-1}) obtained from (b). The contour interval varies for clarity of presentation.

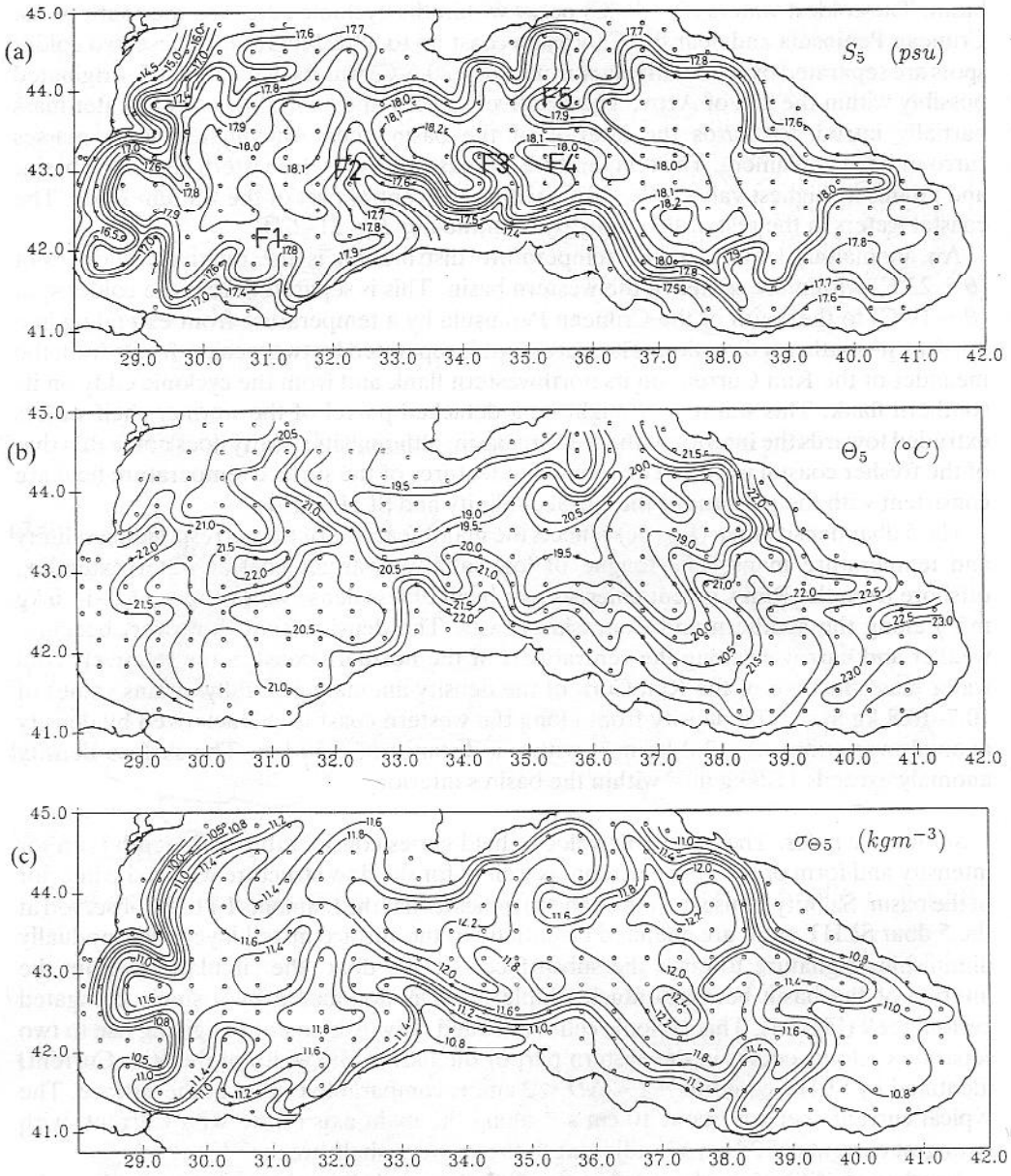

Fig. 5. (a) Salinity at 5 dbar level; (b) potential temperature (°C) at 5 dbar level; (c) σ_θ (kg m^{-3}) at 5 dbar level. The contour interval varies for clarity of presentation.

which is present in the near-surface circulation field of the main part of the Rim Current (cf. Fig. 4a).

At 250 dbar, the Rim Current is still discernible (Fig. 9b), but the intensity of the flow has decreased by a factor of 5–10 compared to the surface. Typical current speed along the main axis of the Rim Current is about 3–4 cm s^{-1}, with a maximum value of 7 cm s^{-1} being

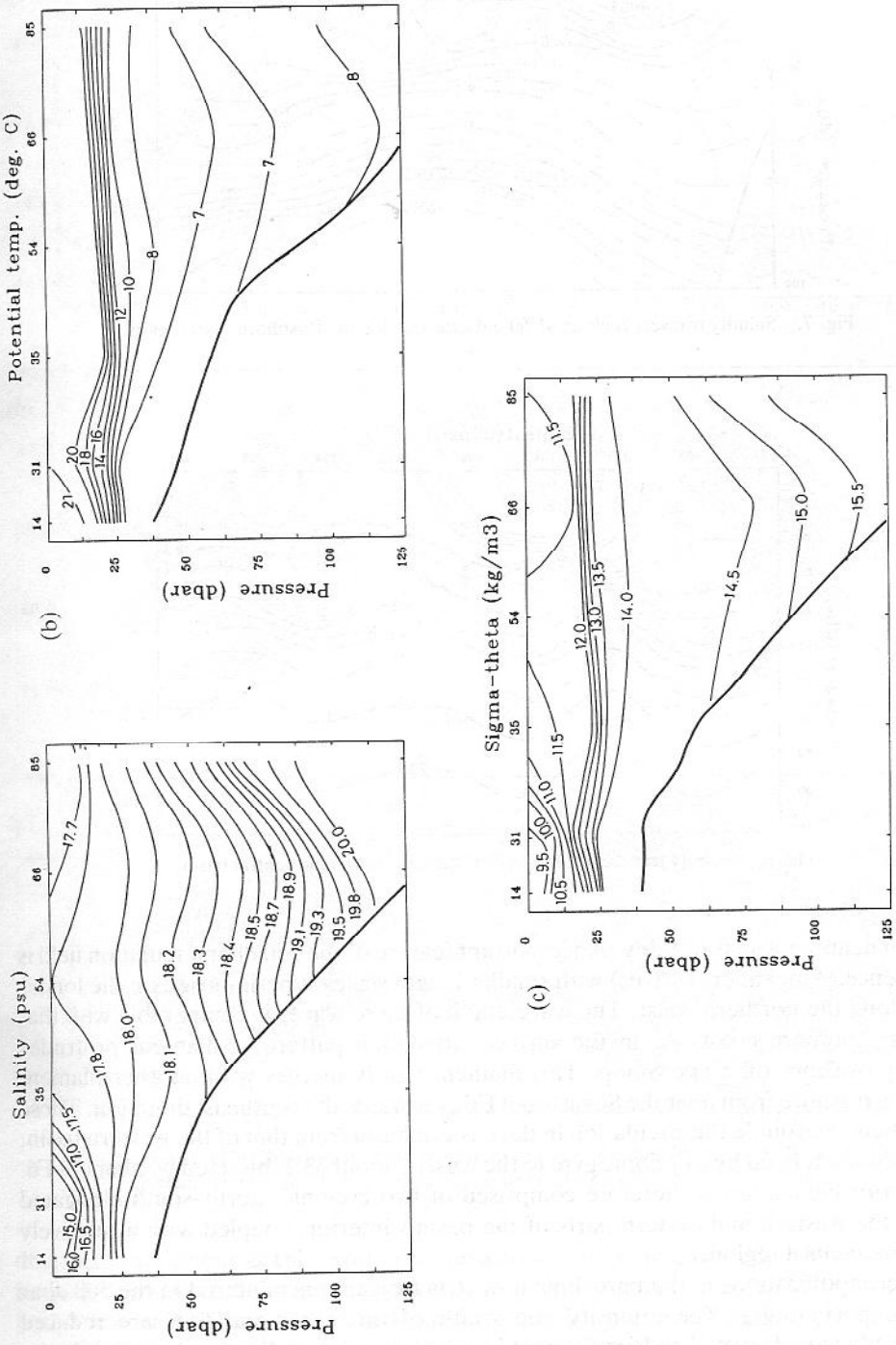

Fig. 6. Transect A extending from the Romanian coast eastward into the Black Sea. (a) Salinity; (b) potential temperature (°C); and (c) σ_θ (kg m^{-3}).

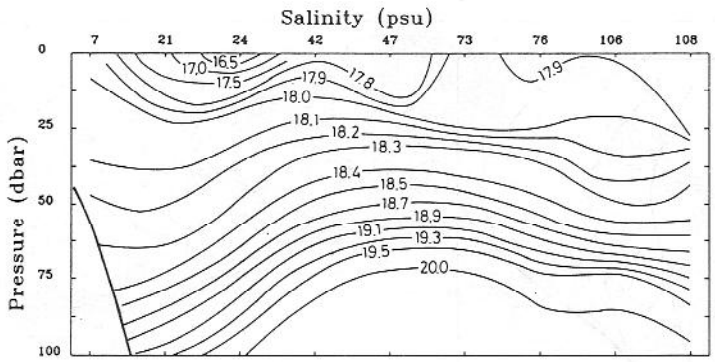

Fig. 7. Salinity transect B along 41°50′ latitude outside the Bosphorus exit region.

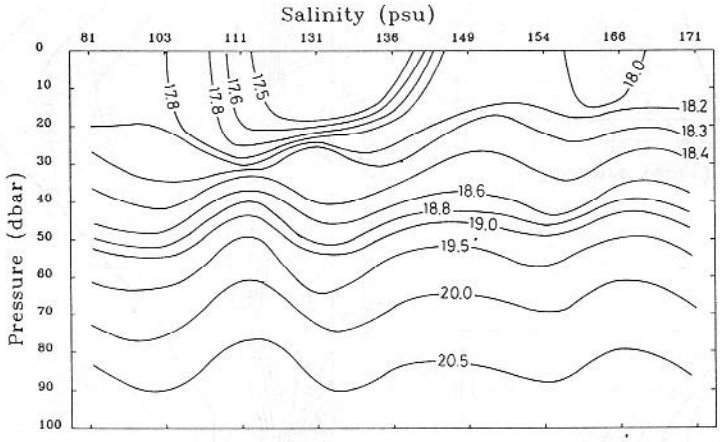

Fig. 8. Salinity transect C along 42°50′ latitude across the central basin.

observed near the Kaliakra Eddy. An important feature of the 250 dbar circulation field is the presence of meanders (waves) with smaller length scales superimposed on the longer waves along the northern coast. The wavelength of these waves is comparable with that along the southern coast. As in the surface circulation pattern, a filament protrudes obliquely offshore off Cape Sinop. This filament nearly merges with another filament extending offshore from near the Sevastopol Eddy towards the southeast direction. These two filaments decouple the circulation in the eastern basin from that of the western basin, which is characterized by a cyclonic gyre to the west of about 33°E bisected by filament F6. The interior circulation is therefore comprised of two cyclonic, north–south elongated gyres in the western and eastern parts of the basin's interior, coupled with a relatively featureless central region.

Further modifications in the baroclinic flow structure are encountered in the 500 dbar SLHT map (Fig. 9c). The intensity and width of the peripheral flow are reduced considerably at this level. The Rim Current is only discernible at this level at a maximum speed of approximately 2 cm s^{-1}. The two filaments of the central basin observed at the 250

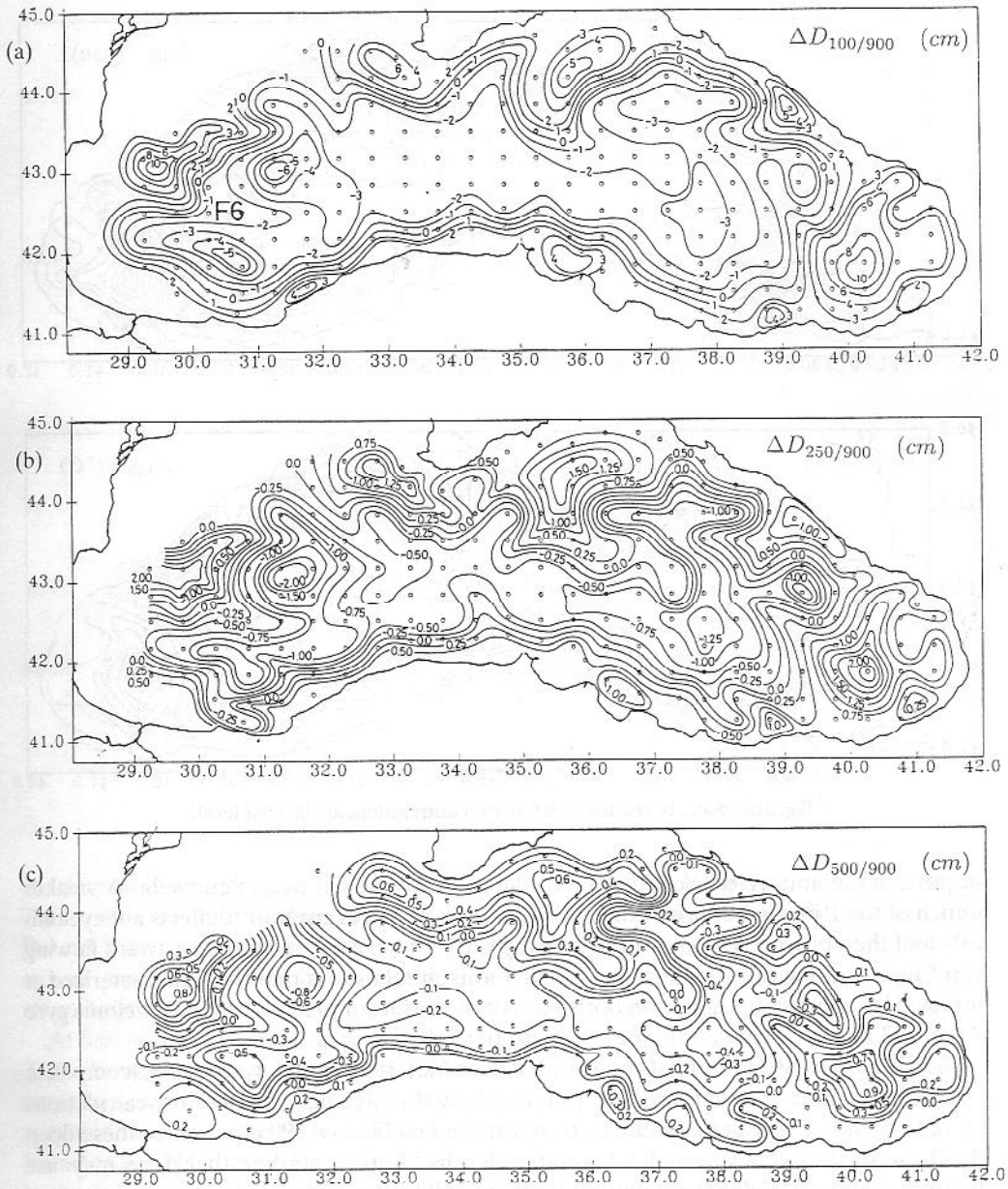

Fig. 9. Sea-level height anomaly maps (cm) relative to the 900 dbar level. (a) At 100 dbar; (b) at 250 dbar; and (c) at 500 dbar. The contour interval varies for clarity of presentation.

dbar field are absent at this level. The Sevastopol and Crimean Eddies have combined, forming an east–west elongated anticyclonic cell covering the northern half of the central basin between 32°E and 37°E. The Rim Current flowing eastward parallel to the southern coast circulates around the periphery of the cyclonic gyre of the eastern basin, splitting into two branches within the central basin along ~35°E. The main branch flows northwestward

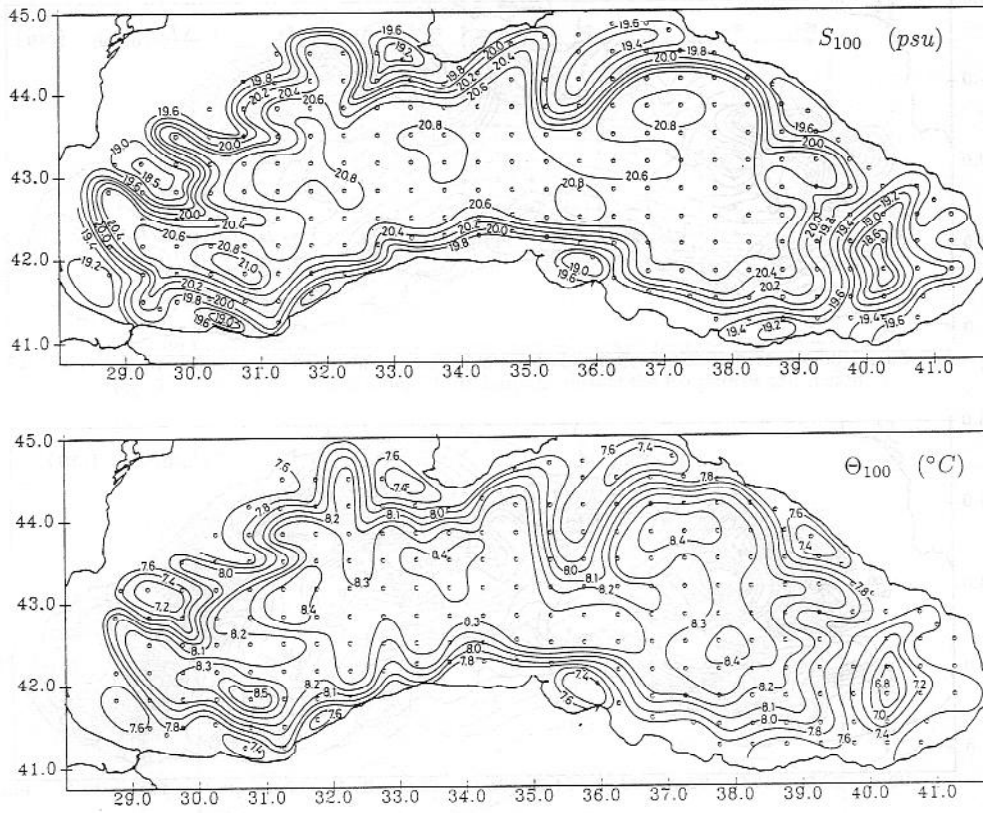

Fig. 10. Salinity and temperature (°C) distributions at 100 dbar level.

supporting the anticyclonic circulation to the south of the Crimean Peninsula. A weak branch of the Rim Current, identified by the $\Delta D = -0.1$ cm contour, deflects anticyclonically and then proceeds west–northwest only ~20–30 nm away from the eastward flowing Rim Current along the southern coast. The basin circulation is therefore characterized at this level by two cyclonic gyres on both sides of the basin coupled with an anticyclonic gyre at the middle.

The 750 dbar SLHT map (not shown) does not reveal any systematic, compos peripheral cyclonic circulation. Experiments show that dynamic topography calculatio are only weakly dependent on choice of reference level below 500 dbar, since these de SLHT anomalies are so small at greater depths. Future studies therefore may u shallower (about 500 dbar) compensation levels with little error.

The salinity and temperature distributions at the subsurface levels also correlate w corresponding dynamic height fields. As in the surface level, the only major differences the two intense meanders of the frontal zone on both sides of the Kaliakra Eddy. At dbar, waters in the Rim Current are identified by a salinity range between 19.8 and 20 and a temperature range between 7.8 and 8.2°C (Fig. 10). The salinity of the inshore ar is less than 19.8, with values decreasing to ~18.5 in the Batumi and Kaliakra Eddi ~18.8 in the Sevastopol Eddy, and ~19.0 in the smaller eddies along the southern coa This peripheral salinity structure creates more than 1 unit salinity difference betwe

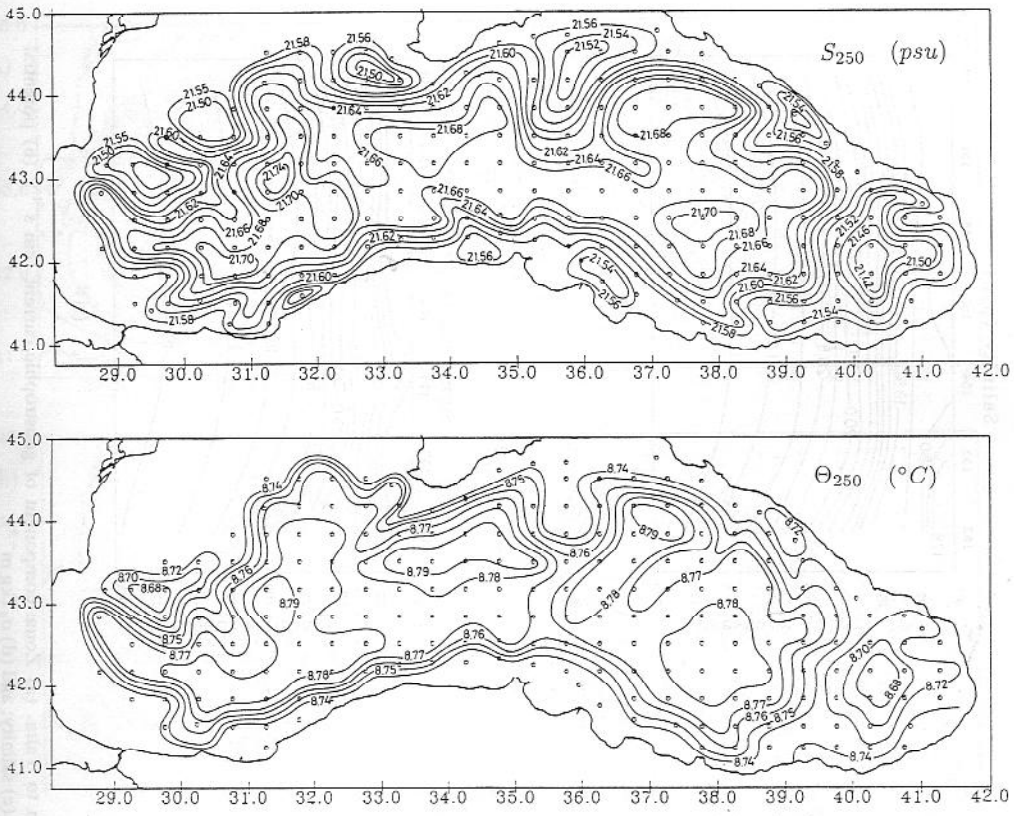

Fig. 11. Salinity and temperature (°C) distributions at 250 dbar level.

coastal and offshore regions. The coastal anticyclonic eddies have temperatures less than 7.6°C, with minimum values of approximately 6.8°C observed within the center of the Batumi Eddy, whereas the interior attains a nearly uniform value of about 8.3°C. The coastal frontal zone and its inshore region around the basin therefore reveal the CIL characteristics at this level.

At 250 dbar, the Rim Current is distinguished by salinity values between 21.58 and 21.66, increasing to a maximum of 21.74 within the interior (Fig. 11a). Coastal areas in the south have salinities between 21.58 and 21.54, and lower salinities are observed within the major anticyclonic eddies: ~21.40 in the Batumi and Kaliakra Eddies, and ~21.50 in the Sevastopol and Crimean Eddies. The frontal salinity structure extending from the surface to the 250 dbar level is no longer apparent in the 500 dbar level, where the salinity varies between two extreme values of 21.98 and 22.06 throughout the entire basin. At 250 dbar, the temperature ranges from ~8.80°C within the cyclonic eddies to ~8.70°C within the coastal waters and the anticyclonic eddies (Fig. 11b). Intrusion of relatively colder waters from the northern coast through the filament F5 is also depicted in both 100 and 250 dbar temperature maps.

The meridional cross-sections of temperature, salinity, density anomaly and the zonal component of the geostrophic current between Sinop and Yalta (along 34°15′E) show further details of the cross-jet properties of the Rim Current (Fig. 12). Along the southern

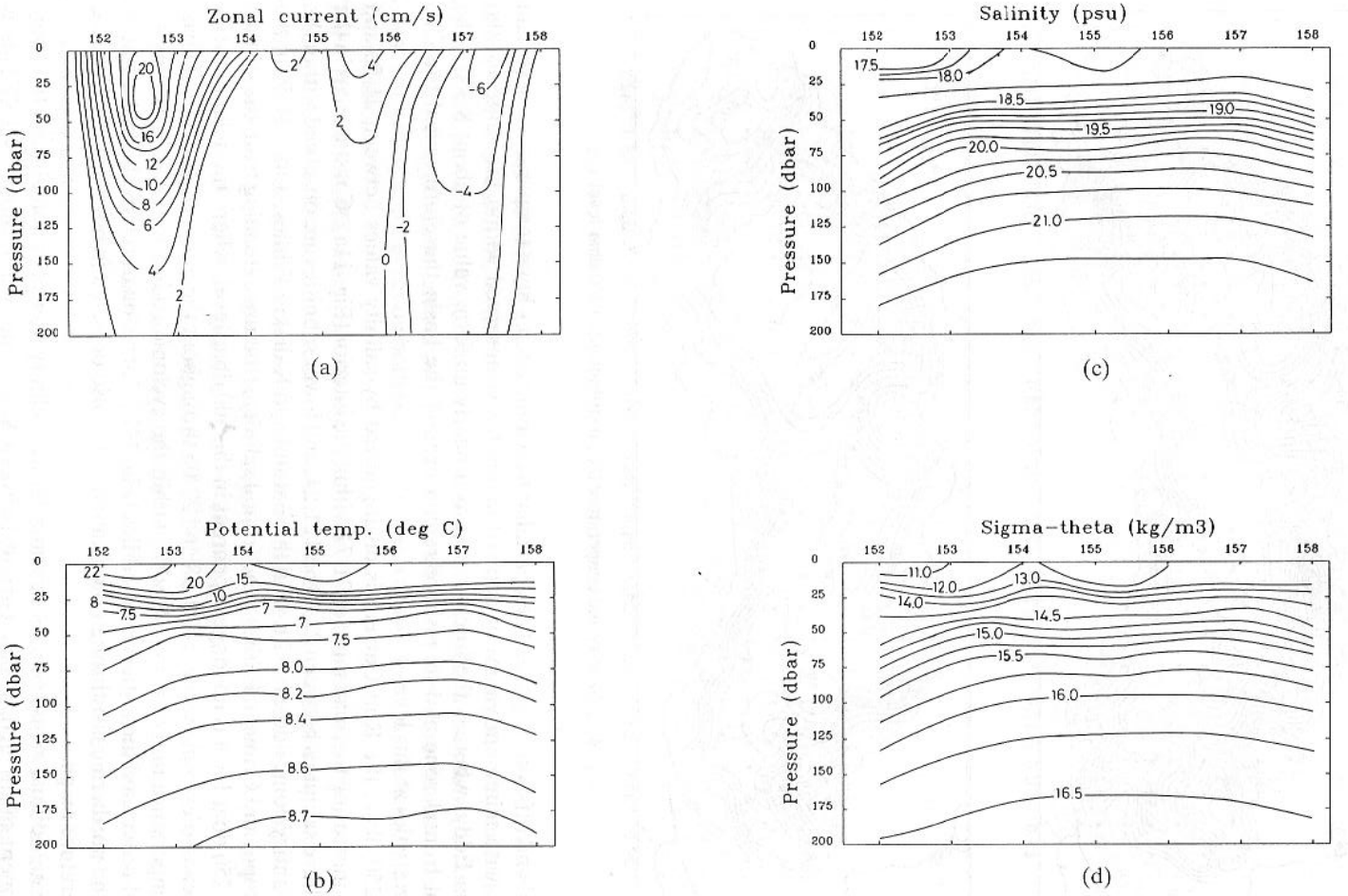

Fig. 12. Meridional transect D (34°15′E) from Cape Sinop north to Yalta. (a) Zonal component of geostrophic current (cm s^{-1}); (b) potential temperature (°C); (c) salinity; and (d) σ_θ (kg m^{-3}).

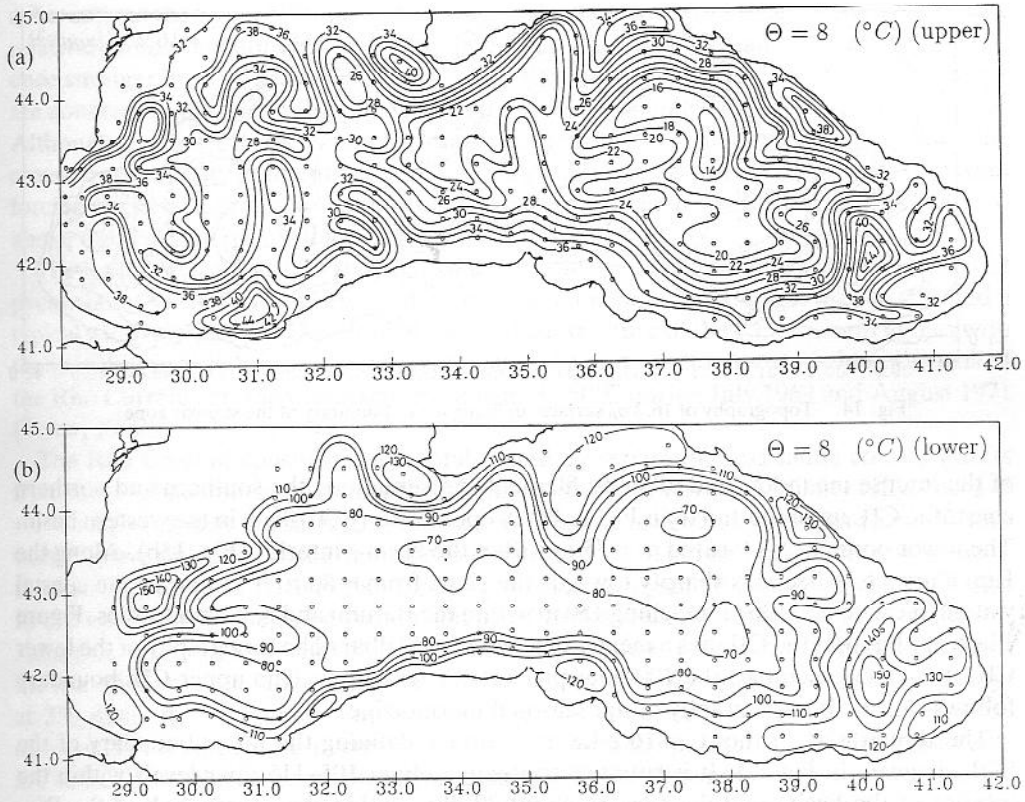

Fig. 13. Cold intermediate layer surfaces defined by 8°C isotherms. (a) Surface of CIL (dbar); and (b) base of CIL (dbar).

coast, the coastal jet has a width of ~75 km, and in the shallow layer above the seasonal thermocline, it is separated from the interior by temperature, salinity and density fronts, with differences of ~2°C, ~0.75 and ~1 kg m^{-3}. The speed of the jet decreases with depth from about 20 cm s^{-1} near the surface to less than 10 cm s^{-1} at ~100 dbar and 2 cm s^{-1} at ~250 dbar. A similar but weaker coastal current system flowing in the opposite direction is shown along the northern coast. Weaker currents are due to the neglect of the meridional component of the jet along this section (see Fig. 4c). The interior region, separated from these two coastal currents by sharp horizontal current shear, is characterized by much weaker currents (<2 cm s^{-1}). Slightly warmer and less saline water and current reversals observed near-surface in the vicinity of Sta. 155 are associated with filament F4 observed in the 5 dbar property fields. Below the seasonal thermocline–halocline–pycnocline system, the isotherms, isohalines and isopycnals slope downward towards both the southern and northern coast, giving rise to the thermohaline dome within the interior, consistent with the horizontal circulation patterns.

Horizontal variability in the upper and lower boundaries of the CIL (Fig. 13) show that the position of the upper boundary varies between 30 and 36 m along the Rim Current (Fig. 13a). It is located at deeper levels (~40 m) within the anticyclonic eddies, and at shallower levels (~20 dbar) within the interior of the eastern and central basins. As a result

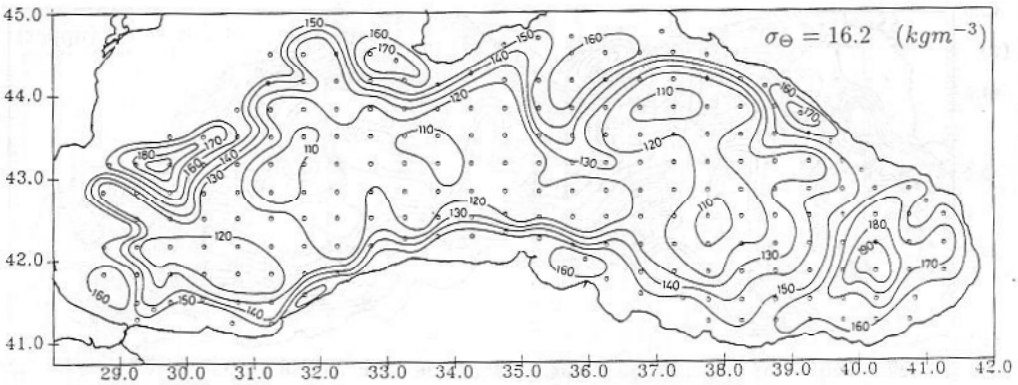

Fig. 14. Topography of 16.2 σ_θ surface, defining lower boundary of the suboxic zone.

of the intense meanders and offshore filaments present along the southern and northern coast, the CIL upper boundary is located at deeper levels (~30 dbar) in the western basin. The lower boundary is located at ~75 m within the basin's interior (Fig. 13b). Along the Rim Current, it deepens sharply towards the coast from ~80 to ~110 m. In the coastal waters, it exceeds ~120 m, reaching 150 m within the Batumi and Kaliakra Eddies. Figure 13a,b implies that the CIL has a mean thickness of ~50 dbar. The topography of the lower CIL boundary resembles the 100 dbar property distributions. The upper CIL boundary follows closely the topography of the seasonal thermocline.

The topography of the $\sigma_\theta = 16.2$ kg m^{-3} surface defining the lower boundary of the SOL, is given in Fig. 14. It is situated approximately at 105–115 dbar levels within the interior of the basin, and deepens by about 30 dbar within the narrow belt of the Rim Current system, and even more within the coastal anticyclonic eddies. Its deepest position is found within the central gyres of the Batumi and Kaliakra Eddies (190 dbar). Recalling that the upper surface of the SOL coincides approximately with the lower boundary of the CIL, Fig. 13b then describes the horizontal variations in the upper SOL surface.

4. DISCUSSION AND CONCLUSIONS

Hydrographic measurements carried out during September 1991 with the participation of five ships from four riparian countries clarify the basin-wide characteristics of the circulation and thermohaline structure of the Black Sea during the late summer season. The data indicate that the three-dimensional flow structure reveals pronounced mesoscale variability. The Rim Current emerges as a dynamic region with surface-intensified (upper 150 dbar) geostrophic flow (core velocities >20 cm s^{-1}). It exhibits large meanders and coast-originating filaments that produce lateral mixing and interleaving in the thermohaline fields. The origin of the meanders is not fully understood, but baroclinic Rossby waves and instabilities associated with them could be possible sources. The inshore part of the Rim Current confined along the steep continental slope appears only marginally unstable and has the form of uniform, small amplitude undulations whose growth may be inhibited by the steep topography. CHAO (1990), for instance, has shown that the bottom slope reduces the cross-isobath movement of currents, and hence their instability, by virtue of potential vorticity conservation. These undulations along the Rim Current are observed

coherently in the upper 500 dbar. The offshore flank of the Rim Current located along the relatively smooth continental margin topography, on the other hand, appears to experience stronger instabilities which spawn meanders and filaments. Some of these filaments are confined to the shallow surface mixed layer whereas others extend to greater depths. Although the deep features may extract their energy from the potential energy of the cross-stream density gradient and kinetic energy of the cross-stream shear, the local wind forcing might be a predominant mechanism for formation of shallower features confined above the seasonal pycnocline.

The intensity and width of the Rim Current reduce considerably below the permanent pycnocline. At 500 dbar, it is only discernible as a maximum current of ~2 cm s^{-1}, and a typical width of ~20 km. This form of the vertical structure of the Rim Current agrees with the monthly current measurements performed at a buoy station located along the axis of the Rim Current, off the Caucasian coast near 37°50′E during July 1969 and August 1971 (Titov, 1980).

The Rim Current constitutes a frontal boundary separating less saline coastal waters from more saline interior waters with cross-frontal temperature and salinity differences of ~1°C and ~0.5 near the surface. Rim Current waters are generally warmer than offshore waters above the seasonal thermocline, but relatively cooler in the subsurface levels due to the advection of the CIL over the inshore 100 km zone around the periphery of the basin. In the upper layer, the intensity and shape of fronts resemble those at the sea surface. Across the pycnocline (~100 dbar), the frontal intensities decrease with depth although the frontal shapes tend to be retained. The decrease is faster for temperature than salinity; at 250 dbar, frontal salinity and temperature gradients are ~10% and ~1% of those observed at the surface, respectively. At 500 dbar both temperature and salinity gradients are so weak that the fronts are hardly discernible. The shallowness of the fronts above the pycnocline may imply important contribution of surface heat and salt fluxes in the formation of the three-dimensional thermohaline structure and associated surface-intensified baroclinic flow.

Along the western shelf/slope boundary, the low salinity shelf water encounters more saline and denser water of the Rim Current and basin's interior. The strong density difference (>2 kg m^{-3}) of these two water masses creates a horizontal density gradient that drives an along-front geostrophic flow which ultimately carries the estuarine water downstream along the shelf break. Combination of the buoyancy-induced current in the shelf and the Rim Current along the topographic slope produces the strongest current in the basin (~0.3 cm s^{-1} at the surface). This frontal system, one of the most persistent features of the thermohaline structure, can be easily identified in satellite imagery as a continuous band of cold surface water along the front (e.g. Oguz *et al.*, 1992). It is especially pronounced during winter when the shelf waters are exceptionally cool (<5°C) (Tolmazin, 1985).

The coastal zone has a series of anticyclonic eddies, most of which have been identified earlier (e.g. Oguz *et al.*, 1993), supporting their existence as quasi-permanent features of the summer circulation. The circulation within the interior of the sea is composed of an interconnecting series of cyclonic eddies and gyres, changing in size and shape with depth. The mesoscale variability introduces complexity to the general circulation at each pressure level, although the larger scale features of the general circulation may be regarded as fairly coherent down to 500 dbar. Important structural changes, however, take place at both large scale and mesoscale components of circulation at 500 dbar and deeper. This feature

of the circulation is consistent with the findings of the September 1990 survey (OGUZ *et al.*, 1993), and also supported to some extent by a series of monthly current measurements (TITOV, 1980) performed at six different buoy stations along the Caucasian coast (located between 37°30′E and 40°23′E). However, the flow structure at or below 500 dbar will remain largely conjectural until long-period current measurements of the order of few years and Lagrangian drifter measurements are made available.

Among the densely populated mesoscale eddies in the basin, two dipole eddy systems are particularly notable in the property distributions. One eddy is situated along the northern coast, off the Sea of Azov (Fig. 15). Its elements are the Crimean anticyclonic eddy and the cyclonic eddy near the northern coast of the eastern basin gyre. They are coupled by the Rim Current and filament F5, forming the stem and the cap of the mushroom eddy system, respectively. Satellite imagery (AVHRR) extending from 10 September through 24 September demonstrates the persistence of this feature throughout the survey period (e.g. Fig. 15). The other dipole eddy is formed by the Kaliakra anticyclonic eddy and the cyclonic eddy near the western coast of the basin with Filament F6 forming the cap of the mushroom eddy system. This feature is apparently a subsurface structure absent within the shallow surface mixed layer. Contrary to near-surface characteristics of the majority of the dipole eddies observed in the literature, they are deep structures and extend to intermediate depths. These two dipole eddies are best shown in the 100 and 250 dbar SLHT maps (Fig. 9a,b), as well as in the corresponding salinity and temperature fields. In addition to these clear dipole structures, the cyclonic–anticyclonic eddy pair together with filament F1 found along the southern coast centered at 30.5°E may form another dipole structure at near-surface levels (see Fig. 4a).

As inferred from the surface dynamic topography map, the Rim Current contains 17 meanders around the basin having wavelengths of ~125 km along the western and southern coast, and having wavelengths of ~250 km along the northern coast. These northern features are further superimposed by shorter waves at intermediate depths. The spatial periodicity of 125 km is consistent with the gravest mode-waves estimated by two-layer baroclinic instability analysis (MYSAK *et al.*, 1977) as well as those carried out by BLATOV and UL'YANOVA (1985) for the average flow and stratification conditions of the Black Sea. Spacing is also in accord with linear theory of small amplitude waves, which predicts wavelengths of $2\pi R = 125$ km (where $R \sim 20$ km is the deformation radius) for perturbations on an unstable current system (KILLWORTH *et al.*, 1984). These features of the Rim Current, however, require further quantitative investigation.

The topography of $\sigma_\theta = 15.4$–15.65 kg m^{-3} and $\sigma_\theta = 16.2$ kg m^{-3} surfaces, defining the upper and lower boundaries of the suboxic layer (SOL), may provide an indirect but more precise way to locate oxygen-deficient levels of the water column when the oxygen and sulfide concentrations are too low, O(10 μm), to be measured with sufficient accuracy using conventional techniques (SAYDAM *et al.*, 1993). The thickness of the SOL in which the DO and H_2S concentrations are low and subject to uncertainties is ~50 dbar. This implies that determination of the position of the anoxic interface is bound to have errors depending on the accuracy of the measurements and the methodology followed by the laboratories participating in this multi-ship operation. In HydroBlack '91, our experience shows this error to be about +10 dbar, varying randomly from station to station, and therefore resulting in a different anoxic interface distribution map as compared to the $\sigma_\theta = 16.2$ kg m^{-3} level map. The postulated rise of the anoxic layer during the last several decades will lie within the uncertainty of the measurements, using conventional sampling.

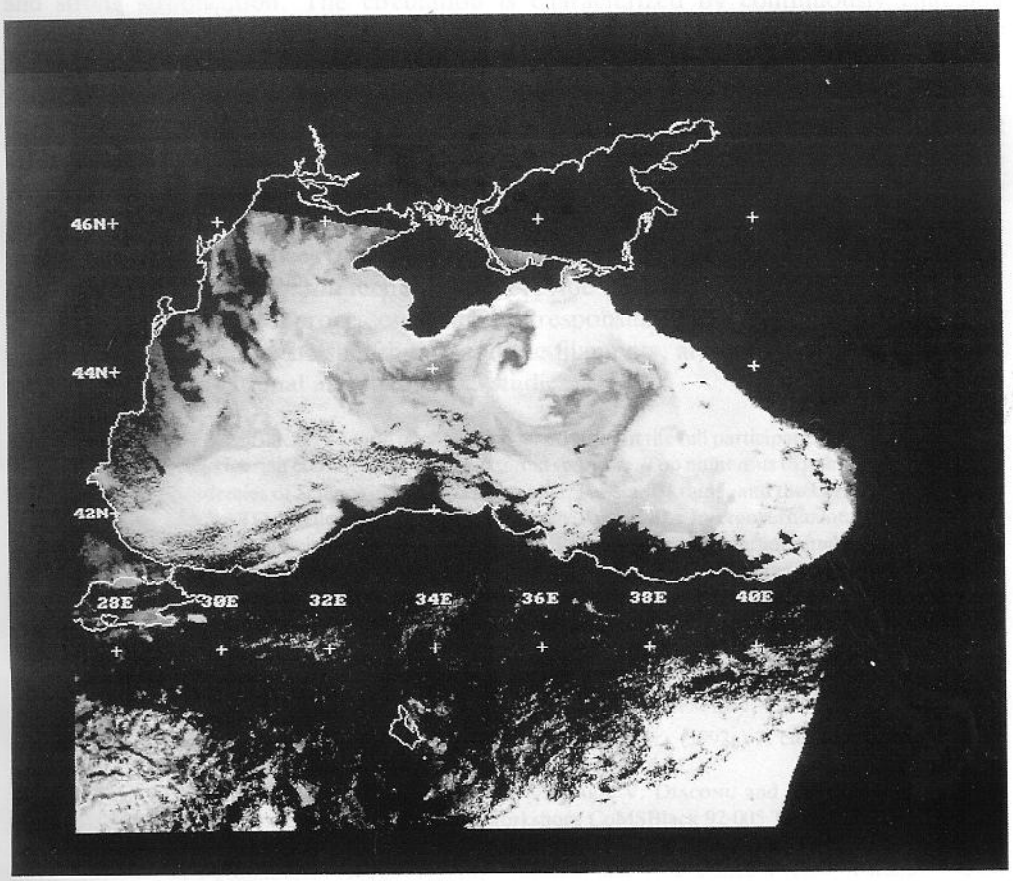

Fig. 15. AVHRR image from the NOAA 10 satellite for 15 September 1991, demonstrating surface temperature contrasts which accompany the mushroom eddy structure south of the Sea of Azov.

This important issue may be resolved more precisely by comparing the topography of 16.2 kg m^{-3} density anomaly maps constructed from existing CTD surveys.

This study, together with the findings from the satellite observations examined both here and reported in OGUZ *et al.* (1992), suggests that the Black Sea circulation is dominated by spatially and temporally evolving meanders and mesoscale eddies. The circulation is in the process of continuous evolution by meanders, vortex dipoles, and offshore jets generated by internal dynamical processes associated with the Rim Current and strong stratification. The circulation is characterized by continuously changing mosaics of cellular patterns within the interior of the basin and throughout the water column.

Much more, however, remains to be studied on the specific details of the three-dimensional flow structure via carefully planned future process-oriented hydrographic surveys and mathematical models. In particular, the temporal and spatial variability, the growth rates, lifetimes and migration of meanders and eddies need to be elucidated by means of direct measurement techniques (e.g. drifters), and numerical model studies. Sea surface elevation differences of O(20 cm) estimated here may be monitored in the future by satellite altimeters or *in situ* techniques to provide time variations of the flow structure in the Black Sea. Frontal processes, which are responsible for oceanic mixing processes taking place both across the shelf break and the filaments, are not fully understood and await further observational and theoretical studies.

Acknowledgements—HydroBlack '91 would not have happened without the full participation of the governments of the various Black Sea riparian countries, as well as external sponsors. Too numerous to name in full, we would like to identify the Academies of Science in Bulgaria, Romania, Russia, Ukraine, and the United States, as well as the TUBITAK and NATO Science for Stability Program in Turkey, the Intergovernmental Oceanographic Commission, and the National Science Foundation for U.S. Participation under grant number OCE-9121788. Significant private contributors to this effort include the Regional Environmental Center for Central and Eastern Europe, the Andrew W. Mellon Foundation, and the Woods Hole Oceanographic Institution (through its Director, Craig Dorman). This is CoMSBlack-009 publication number.

REFERENCES

AUBREY D. G., Z. BELBEROV, A. BOLOGA, V. EREMEEV and Ü. ÜNLÜATA (1992a) A coalition to diagnose the patient: CoMSBlack and the Black Sea. *Marine Technology*, **2**, 5–8.

AUBREY D. G., T. OGUZ, E. DEMIROV, V. IVANOV, T. MCSHERRY, V. DIACONU and E. NIKOLAENKO (1992b) HydroBlack 91: Report of the CTD calibration workshop. CoMSBlack 92-005 Technical Report. Woods Hole Oceanographic Institution Technical Report WHOI-92-10, CRC-92-01, 126 pp.

BLATOV A. S., N. P. BULGAKOV, V. A. IVANOV, A. N. KOSAREV and V. S. TUJILKIN (1984) Variability of the hydrophysical fields in the Black Sea. Hydrometeoizdat, Leningrad, 249 pp. (In Russian).

BLATOV A. S. and V. I. UL'YANOVA (1985) Effect of curvature of vertical velocity and density profiles on the hydrodynamic stability of a zonal flow. *Oceanology*, **25**, 11–16.

CHAO S-YU (1990) Instabilities of fronts over a continental margin. *Journal of Geophysical Research*, **95**, 3199–3211.

EREMEEV V. N., L. M. IVANOV, A. D. KIRWAN JR, O. V. MELNICHENKO, S. V. KOCHERGIN and R. R. STANICHNAYA (1992) Reconstruction of oceanic flow characteristics from quasi-Lagrangian data, 2: characteristics of the large scale circulation in the Black Sea. *Journal of Geophysical Research*, **97**, 9743–9753.

EREMEEV V. N., L. M. IVANOV, S. V. KOCHERGIN and O. V. MELNICHENKO (in press) Seasonal variability and types of currents in the upper layer of the Black Sea. *Soviet Journal of Physical Oceanography*.

FILIPPOV D. M. (1968) *Circulation and water masses in the Black Sea*. Nauka Publishing, Moscow, 260 pp. (In Russian).

IVANOV V. A., A. S. KUKUSHKIN and A. S. SAMODUROV (1985) Sixth cruise of the R/V Prof. Kolesnikov in the Aegean Sea and Black Sea (June 24, August 25, 1983). *Oceanology*, **25**, 278–281.

Izdar E. and J. W. Murray (1992) *Black Sea oceanography*. NATO ASI Series, Kluwer Academic Publ Dordrecht, 487 pp.

Kazmin A. and V. Skliarov (1982) Some peculiarities of the Black Sea circulation inferred from the N Satellite. *Investigation of the Earth from Space*, **6**, 42–49. (In Russian).

Killworth P. D., N. Paldor and M. E. Stern (1984) Wave propagation and growth on a surface front in layer geostrophic current. *Journal of Marine Research*, **42**, 761–785.

Latif M. A., E. Özsoy, T. Oguz and Ü. Ünlüata (1991) Observations of the Mediterranean effluent Black Sea. *Deep-Sea Research*, **38**, Suppl. 2, S711–S723.

Latun V. S. (1990) Anticyclonic eddies in the Black Sea in summer of 1984. *Soviet Journal of P Oceanography*, **1**, 279–286.

Mee L. D. (1992) The Black Sea in crisis: the need for concerted international action. *Ambio*, **21**, 278–2

Murray J. W. (1991) Black Sea Oceanography: Results from the 1988 Black Sea Expedition. *De Research*, **38**, Suppl. 2.

Murray J. W., L. A. Codispoti and G. E. Friederich (in press) Redox Environments: the suboxic zone Black Sea. In: *Aquatic chemistry*, C. P. Huang, C. R. O'Melia and J. J. Morgan, editors, Am Chemical Society.

Murray J. W., Z. Top and E. Özsoy (1991) Hydrographic properties and ventilation of the Black Sea. *De Research*, **38**, Suppl. 2, S663–S690.

Mysak L. A. (1977) On the stability of the California undercurrent off Vancouver Island. *Journal of P Oceanography*, **7**, 904–917.

Oguz T., M. A. Latif, H. I. Sur, E. Özsoy and Ü. Ünlüata (1991) On the dynamics of the southern Blac In: *Black Sea oceanography*, NATO ASI series C-Vol. 351, E. Izdar and J. W. Murray, editors, K Dordrecht, pp. 43–64.

Oguz T. and L. Rozman (1991) Characteristics of the Mediterranean underflow in the southwestern Bla continental shelf/slope region. *Oceanologica Acta*, **14**, 433–444.

Oguz T., P. La Violette and Ü. Ünlüata (1992) The upper layer circulation of the Black Sea: Its variab inferred from hydrographic and satellite observations. *Journal of Geophysical Research*, **97**, 12569–1

Oguz T., V. S. Latun, M. A. Latif, V. V. Vladimirov, H. I. Sur, A. A. Markov, E. Özsoy, Kotovshchikov, V. V. Eremeev and Ü. Ünlüata (1993) Circulation in the surface and intermediate of the Black Sea. *Deep-Sea Research I*, **40**, 1597–1612.

Özsoy E., Z. Top, G. White and J. W. Murray (1991) Double diffusive intrusions, mixing and deep conv processes in the Black Sea. In: *Black Sea oceanography*, NATO ASI series C-Vol. 351, E. Izdar and Murray, editors, Kluwer, Dordrecht, pp. 17–42.

Sapozhnikov V. V. (1991) Biohydrochemical barrier on the outer margin of shelf waters of the Blac *Oceanology*, **31**, 417–423.

Saydam C., S. Tugrul, O. Basturk and T. Oguz (1993) Identification of the oxic/anoxic interface by iso surfaces in the Black Sea. *Deep-Sea Research I*, **40**, 1405–1412.

Sorokin Y. I. (1982) *The Black Sea*. Nauka Publishing, Moscow, 217 pp. (In Russian).

Stanev E. V., D. I. Troukhchev and V. M. Roussenov (1988) *The Black Sea circulation and numerical mo of the Black Sea currents*. Sofia University Press, Sofia, 222 pp. (In Russian).

Titov V. B. (1980) Character of the circulation and vertical structure of currents in the eastern part of the Sea. *Oceanology*, **20**, 279–282.

Tolmazin D. (1985) Changing coastal oceanography of the Black Sea, I: Northwestern shelf. *Prog Oceanography*, **15**, 217–276.

Trukhchev D. I. and Y. L. Demin (1992) The Black Sea general circulation and climatic temperature and s fields. CoMSBlack 92-010 Technical Report. Woods Hole Oceanographic Institution Technical R WHOI-92-34, CRC-92-02, 132 pp.

Tugrul S., O. Basturk, C. Saydam and A. Yilmaz (1992) Changes in the hydrochemistry of the Bla inferred from water density profiles. *Nature*, **359**, 137–139.

Vinogradov M. Y., E. I. Musayeva and T. N. Semenova (1990) Factors determining the position of the layer of mesoplankton concentration in the Black Sea. *Oceanology*, **30**, 217–224.